



Published in final edited form as:

Nat Commun. ; 5: 4173. doi:10.1038/ncomms5173.

Evidence for an electrostatic mechanism of force generation by the bacteriophage T4 DNA packaging motor

Amy D. Migliori^{a,*}, Nicholas Keller^{a,*}, Tanfis I. Alam^b, Marthandan Mahalingam^b, Venigalla B. Rao^{b,**}, Gaurav Arya^{c,**}, and Douglas E Smith^{a,**}

^aDepartment of Physics, University of California, San Diego, 9500 Gilman Drive, La Jolla, CA 92093-0379

^bDepartment of Biology, The Catholic University of America, 620 Michigan Ave. NE, Washington, DC, 20064

^cDepartment of NanoEngineering, University of California, San Diego, 9500 Gilman Drive, La Jolla, CA 92093

Abstract

How viral packaging motors generate enormous forces to translocate DNA into viral capsids remains unknown. Recent structural studies of the bacteriophage T4 packaging motor have led to a proposed mechanism wherein the gp17 motor protein translocates DNA by transitioning between extended and compact states, orchestrated by electrostatic interactions between complimentary charged residues across the interface between the N- and C-terminal subdomains. Here, we show that site-directed alterations in these residues cause force dependent impairments of motor function including lower translocation velocity, lower stall force, and higher frequency of pauses and slips. We further show that the measured impairments correlate with computed changes in free energy differences between the two states. These findings support the proposed structural mechanism and further suggest an energy landscape model of motor activity that couples the free energy profile of motor conformational states with that of the ATP hydrolysis cycle.

Introduction

Many double-stranded DNA viruses utilize a powerful molecular motor during assembly to translocate DNA into a preformed capsid shell¹⁻⁶. The motor must do significant mechanical work against forces arising from DNA bending rigidity, electrostatic self-repulsion, and entropy loss, which oppose DNA confinement⁷⁻¹². Measurements of DNA packaging with optical tweezers in bacteriophages $\phi 29$, λ , and T4 show that all three motors can generate

Users may view, print, copy, and download text and data-mine the content in such documents, for the purposes of academic research, subject always to the full Conditions of use:http://www.nature.com/authors/editorial_policies/license.html#terms

**Corresponding authors: Douglas E. Smith (des@ucsd.edu), Gaurav Arya (garya@ucsd.edu), Venigalla B. Rao (rao@cua.edu).

*These authors contributed equally

Author Contributions: D.E.S., G.A., and V.B.R. designed research, A.D.M. performed the molecular dynamics simulations, free energy calculations, preliminary experiments, and data analysis with assistance from D.E.S and G.A. N.K. performed experiments and data analysis with assistance from D.E.S. T.I.A. and M.M. prepared T4 components. D.E.S., G.A., and A.D.M. wrote the paper with assistance from N.K. and V.B.R.

Competing interests: The authors declare no competing interests

forces >50 pN, which is $>20\times$ higher than forces generated by skeletal muscle myosin motors^{1,13,14}. The motors differ in DNA translocation rates, which range from up to ~ 200 bp/s for $\phi 29$ to up to ~ 2000 bp/s for the T4 motor¹³⁻¹⁵.

A number of studies have begun to examine the microscopic details of the motor mechanism. Measurements of single-DNA packaging dynamics of $\phi 29$ via optical tweezers have enumerated the mechanical and chemical kinetic transitions and rate constants, step size, and coordination of motor subunits^{1,16-18}. Bioinformatics analyses and mutagenesis studies altering the λ and T4 motor proteins indicate the presence of several functional motifs that are homologous with the ASCE (additional strand, conserved E) superfamily of ATPases, including the DNA and RNA translocating helicases and chromosome segregating transporters¹⁹⁻²¹. Single-molecule packaging measurements with phage λ showed that mutations in the Walker A, C-motif, Q-motif, and other structurally conserved regions of the large terminase subunit cause phenotypic impairments in motor function, including reduced translocation velocity, increased pausing and slipping, and steepening of the force-velocity relationship^{22,23}. The structure-function relationships for these motors have remained unclear due to lack of high-resolution structures, unlike the situation for other biomotors such as helicases and F1-ATPase where sophisticated structural models have been proposed²⁴⁻²⁶.

The recent determination of a high-resolution X-ray structure of the T4 large terminase subunit (gp17), along with cryo-electron microscopy (EM) reconstruction of the entire prohead-motor complex, has made this system attractive for probing detailed structure-function relationships of viral DNA packaging²⁷. The cryo-EM data indicates that the motor consists of a pentameric ring of gp17 subunits attached to a dodecameric ring of gp20 proteins, together forming the portal entry channel (Fig. 1a). gp17 was found to have globular N- and C-terminal subdomains connected by a flexible linker region. While there has been some debate regarding which subdomain binds to the portal based on studies of several different phages using multiple different techniques²⁸⁻³⁰, fitting of the gp17 crystal structure into the cryo-EM density of the prohead-motor complex suggests that it is the N-terminal subdomain²⁷. Comparisons also revealed two distinct conformations: a “compact” state seen in the X-ray structure of the gp17 monomer in which the N- and C-terminal domains are in close contact, and an “extended” state, seen in the cryo-EM structure of packaging complexes in which the N- and C-terminal domains are separated by ~ 7 Å (previously referred to as “tensed” and “relaxed” states, respectively)²⁷.

Based on the two different conformations of gp17 seen in the structural data, Sun et al.²⁷ proposed a model for motor operation in which the DNA is translocated in ~ 7 Å (≈ 2 bp) increments by the transition of gp17 from the extended to compact state (Fig. 1b). Inspection of the interface between the domains revealed five aligned pairs of complementarily charged residues, which led to the proposal that this transition is driven by electrostatic interactions between these charged residues across the interface that generate force to translocate the DNA into the prohead. ATP hydrolysis was proposed to regulate DNA interaction and provide energy to return gp17 to the extended state after each 2 bp DNA translocation step. We refer to this model as the “electrostatic force model”. Another model for T4 packaging in which the portal grips the DNA and gp17 exerts force that compresses the DNA until the

portal releases it has been proposed³¹. Although many aspects of these models are not mutually exclusive, and several different packaging models describing other systems, including one based on the crystal structure of phage Sf6 large terminase gp2, have been proposed^{3,4,32-36}, the model proposed by Sun et al. is the only one to propose a detailed mechanism implicating specific residues as critical for force generation based on the atomic structure of the motor protein.

Here, we examine the force-generating mechanism of the T4 motor by measurements of single DNA molecule packaging dynamics with increasing applied forces (Fig. 1c) and characterize the effects of mutations that alter charged residues at the interface between the N- and C-terminal subdomains identified in the crystal structure. We also carried out molecular dynamics simulations to predict free-energy difference between the extended and compact states of gp17 and effect of the residue changes. We find that predicted changes in free-energy correlate strongly with measured impairments of motor function, consistent with the electrostatic force model. Our findings suggest a simple mechanochemical energy landscape picture of gp17 motor dynamics that can explain the experimental observations and simulations.

Results

Site directed mutagenesis

To investigate whether the pairs of apparently aligned, complimentary charged residues within the interface domain observed in the gp17 crystal structure are critical to motor function, we used site-directed mutagenesis to alter these residues. Fig. 2a shows the locations of the mutated residues in the motor (see Supplementary Fig. 1 for additional views). We substituted these amino acids with ones with reversed charges (*i.e.*, we changed + to -, or - to +) to weaken the putative attractive electrostatic interactions between the N- and C-terminal subdomains proposed to generate force. In particular, six mutants with single residue changes (K23E, E303K, K305D, E309K, K504E, and E537K) and three with double residue changes (E303K-K504E, E537K-K305D, and E537K-K504E) were studied. Of these, six exhibited little or no packaging activity, as measured in bulk packaging reactions by DNase protection assays (Supplementary Fig. 2). While these findings suggest that these residues play an important role in packaging it is important to note that packaging activity as assessed by only these bulk assays can exhibit impairment for multiple reasons, including failure of motor proteins to fold assemble into active multimeric complexes, or initiate interactions with DNA. Three of the mutants (E303K, E537K, and E537K-K305D), exhibited sufficient activity to permit detailed measurements of packaging dynamics using the single-molecule optical tweezers assay.

Measurements of DNA packaging dynamics at low force

We first carried out single-molecule packaging measurements using the low force clamp technique described previously¹⁴. Briefly, T4 prohead-motor complexes were assembled using purified recombinant gp17, attached to microspheres via antibodies, injected into a fluid chamber containing ATP, and trapped in one optical trap. DNA molecules were biotinylated at one end and attached to streptavidin-coated microspheres and trapped in a

second optical trap. Packaging was initiated by bringing the two microspheres into proximity such that the motor binds to and begins reeling in the DNA, thus exerting a force that pulls the two microspheres together (Fig. 1c). DNA translocation was tracked using a feedback control system that held the applied load force at a constant value of 5 pN, which is low compared to the maximum force generated by the WT motor (>60 pN).

Measurements were made with the three mutants and with wild-type (WT) gp17 for comparison (Fig. 2b). We found that E537K mutants packaged at nearly the same rate (~600 bp/s) on average as WT, while E303K and E537K-K305D mutants showed a modest reduction to ~400 bp/s. The reductions were partly due to an increase in pausing and slipping and partly due to inherently reduced motor velocity (as shown below). These results clearly show that some of the charged residues at the interface play an important role in the DNA translocating function of the T4 motor. However, given that one mutant (E537K) exhibited no measurable change, the other two mutants exhibited only modest changes, and unexpectedly, the double mutant (E537K-K305D) did not show greater impairment, support for the electrostatic force model from these measurements alone could be considered ambiguous.

High force measurements

We next investigated the motor response under increasing applied loads, where the impact of changes in residues putatively involved in force generation would be expected to be greater. In our previous studies of the WT motor, high force measurements were made by holding the trap positions fixed and allowing the tension in the DNA to build up due to the shortening of the DNA tether accompanying packaging¹⁴. This approach is undesirable for characterizing mutants because they package DNA at slower rates, which would cause a slower build-up of force. This would lead to a bias in the comparison of the WT and different, as different complexes would experience different force loading histories. Also, prolonged force build up frequently leads to rapid detachment of the tethered complexes before the target force is reached, due to the DNA slipping out of the prohead or dissociation of the prohead from the antibody-coated microsphere^{14,37}. Therefore, in the present work we implemented a new protocol in which we first packaged ~5 kbp of DNA at low force (5 pN) to confirm activity, and then quickly ramped the force to a higher value and clamped it via feedback control to measure the response of the motor. Thus, all complexes, WT and mutants, were subject to the same force loading history.

Using this new protocol, force clamp measurements were recorded at 5, 15, 30, 40, 50, and 60 pN loads. Examples of individual packaging traces are shown in Fig. 2c,d, highlighting the highly variable and stochastic nature of packaging by the gp17 motor. We also note the presence of pauses in translocation (flat regions) and slippage (negative slope) interspersed with DNA packaging episodes (positive slope). The overall trend is that velocity decreases with increasing applied load, which implies that the rate limiting step in the mechanochemical cycle involves DNA translocation and, hence, mechanical work done by the motor against the load slows down the overall motor velocity³⁸. Mutations further slow packaging and the time spent pausing and slipping also increases with increasing load and mutations. A perhaps unexpected minor feature in the data is the occurrence a similar

average packaging rate at 30 pN and 15 pN and slightly higher % time packaging at 30 pN than at 15 pN. The cause of this behavior is not clear, but it may be related with the observation that the motors sustain the 15 pN load for much longer time (115 sec, on average) than the 30 pN load (32 sec, on average).

We analyzed ensembles of packaging trajectories to determine several averaged metrics of motor function (Fig. 3). Specifically, we calculated the “packaging rate”, defined as the net length of DNA packaged per unit time; the “motor velocity”, defined as the rate of DNA translocation during episodes of packaging (*i.e.*, not including pauses and slips); and the “percent time spent packaging”, defined as the percentage of time packaging occurs (vs. pausing or slipping). All three metrics show that the residue changes cause more severe impairment at high load than at low load. For example, the packaging rate for mutant E303K, which was ~ 400 bp/s at 5 pN, drops below zero at forces ≥ 15 pN. E303K exhibits episodes of packaging, but slips so frequently that there is no net packaging. The packaging rates for E303K and E537K-K305D, which were nearly the same at 5 pN, also exhibited a clear difference at forces ≥ 15 pN. The rate for E537K, which is the same as that of WT at 5 pN, drops below zero at 50 pN whereas the wildtype averages ~ 20 bp/s. Above 30 pN, the percent time packaging for all the mutants drops clearly below that of WT, and at 60 pN it drops to 0% for all the mutants vs. $\sim 12\%$ for WT. At 50 pN the mutants displayed only brief episodes of highly slowed packaging, and at 60 pN no packaging was detected, whereas the WT motor was still able to package with an average motor velocity of ~ 100 bp/s.

Thus, the mutant motors exhibit a reduced force-generation capacity, with F_{\max} between 50 and 60 pN. Overall, these results showed that all of the charged residues altered by mutagenesis play an important role in motor function. These results are consistent with the electrostatic force model because residue changes expected to weaken the electrostatic interactions proposed to drive the extended-to-compact transition indeed cause impairments in the packaging rate and force-generating capacity of the motor.

Molecular dynamics-based free energy calculations

We next sought to investigate more quantitatively how different residue changes would be expected to affect the conformational change of gp17 from the extended to compact states. In particular, we investigated whether the predicted degree of impairment would follow a similar trend as observed in our experimental measurements of impaired function, which increased in the following order: WT, E537K-K305D, E537K, and E303K. To this end, we carried out molecular dynamics (MD) simulations of gp17 to predict the free energy difference G_{EC} between the extended (**E**) and compact (**C**) states observed in the structural studies. Because of the limited structural information for this system, we do not attempt to model the motor-DNA interaction or the full ATP hydrolysis cycle. Thus, our modeling is necessarily more limited compared with the more intricate models that have been developed to understand detailed structure-function relationships for other biomotors such as the large tumor antigen helicase and F1-ATPase, where structures are available in different nucleotide states and for the helicase with DNA bound^{25,26}.

We determined $G_{EC} = G_C - G_E$ by computing the free energies of the compact (G_C) and extended states (G_E) relative to a common reference state. The relative free energies for each

state were calculated as “binding free energies” between the N- and C-terminal domains using the Molecular Mechanics Generalized Born Surface Area (MM-GBSA) approach³⁹. In these calculations, the compact state was modeled as the available crystal structure of gp17 in the compact state while the extended state observed in cryo-EM studies was modeled from the crystal structure by imposing a 7 Å separation between the N- and C-terminal domains.

Our calculations yielded $G_{EC} = -38.21 \pm 4.42$ kcal/mol for WT gp17, -19.95 ± 9.99 kcal/mol for E537K-K305D, -6.14 ± 3.44 kcal/mol for E537K, and -2.79 ± 5.55 kcal/mol for E303K. These values do not include contributions from changes in the configurational (mostly vibrational) entropy of the gp17, as we found that estimates of vibrational entropy from normal mode calculations yielded large uncertainties. We do not, however, expect vibrational entropy to vary significantly across different mutants. Notably the determined free energy values are all negative, consistent with the transition from the extended to compact state being most favorable for the WT gp17 and favorable to a lesser degree for the mutants. We also carried out calculations for the mutant E309K, which exhibited no packaging activity in both bulk packaging assays and optical tweezers assays. Notably for this mutant we calculated a positive or near zero (unfavorable) $G_{EC} = 1.83 \pm 10.3$ kcal/mol.

For WT gp17, the calculated absolute value $|G_{EC}| \cong 38$ kcal/mol is equivalent to ~ 260 pN·nm of energy, which implies that the maximum force that can be exerted during the $x = 0.7$ nm separation change between the N- and C-terminal subdomains is $F_{\max} = |G_{EC}|/x \cong 370$ pN. Thus, our calculations show that the extended-to-collapsed state transition can indeed produce more than enough force to explain the very high measured forces (>60 pN) generated during packaging. The energy released by hydrolysis of one ATP under the experimental conditions is also sufficient to generate 60 pN of force, as discussed previously¹⁴. However, the predicted $|G_{EC}|$ is about twice the ~ 130 pN·nm free energy released by hydrolysis of a single ATP molecule, suggesting hydrolysis would not provide enough energy to return from the compact state to the extended state. However, several caveats regarding the calculations could potentially be responsible for this discrepancy. Due to lack of detailed structural information, we approximate the extended state structure by simply displacing the center-of-mass of the C-terminal domain away from that of the N-terminal domain by 7 Å. In reality, changes in orientations of the domains may affect G_{EC} values⁴⁰. Also, our calculations ignore the other components of the motor complex—neighboring gp17 subunits along with the threaded DNA molecule—whose configuration remains undetermined. These components likely occlude portions of the N- and C-terminal domain interface from getting solvated, causing our calculations to either over- or under-predict the solvation free energy. Our calculations neglect potential contributions from the configurational entropy of gp17 within the full pentameric active complex, as discussed above. Finally, the MM-GBSA approach itself contains several approximations which may introduce inaccuracies in the absolute free energies values⁴¹, and, like all other biomolecular simulations, our calculations are also subject to the inherent inaccuracies in the force field representation of protein, solvent, and ions. For these reasons, we expect the relative trend of changes in G_{EC} with residue changes to be more meaningful than absolute G_{EC} values.

Correlation of measured and computed impairments

To compare the measured and calculated metrics of motor function we calculated the Pearson correlation coefficients (0 = “no correlation”, 1 = “perfect correlation”) between each of the three measured quantities (Fig. 3, right panel), at each of the five increasing values of applied force, and the calculated G_{EC} values for the WT gp17 and three mutants. We observe significant correlations in all cases and the degree of correlation increases with increasing applied force. At 5 pN, the packaging rate and motor velocity correlate only weakly with G_{EC} , but the correlation coefficients increase to 0.88 and 0.96, respectively, at 50 pN. The correlation coefficient for time spent packaging also rises from 0.65 to 0.95 as the force is increased from 5 to 50 pN.

Thus, we have shown that the measured degree of motor impairment due to the residue changes correlates well with the calculated degree of impairment in terms of change in free-energy difference between the extended and compact states of gp17. The strength of correlation increases at high force, where the motor is subject to higher load, consistent with the proposal that the E-C transition is responsible for force generation. Several features, such as the double mutant E537K-K305D exhibiting less impairment than single mutant E303K, are reconciled by these calculations. The measured % times spent packaging and motor velocities also asymptote towards zero with increasing force in the order E303K, E537K, E537K-K305D, WT, consistent with the order of increasing magnitudes of the calculated favorable free-energy changes.

Mechanochemical energy landscape model

Based on our findings above, we propose a minimal free energy landscape model of gp17 mechanochemistry (Fig. 4) that provides additional insights into the dynamics of the phage T4 DNA packaging motor. As discussed before, we do not attempt to model the motor-DNA interactions because of the lack of structural information. In this model, the free energy landscape (G_{tot}) governing gp17 motor function under applied loads is made up of contributions from the intrinsic conformational free energy landscape of gp17 (G_{gp17}), the chemical free energy of ATP during the hydrolysis cycle (G_{ATP}), and the mechanical work performed by gp17 against the applied load during DNA translocation (W), i.e., $G_{tot} = G_{gp17} + G_{ATP} + W$.

We consider the simplest “tight coupling” model in which ATP hydrolysis is assumed to result in one DNA translocation step. The energetics of ATP hydrolysis by motors with structurally homologous ATPase domains has been well characterized and has been shown to consist of two main steps that release energy: the ATP binding and product release steps²⁴. The approximate G_{ATP} profile based on Ref. 24 is sketched as the blue line in Fig. 4b-d; in these conditions, the ATP binding and product release steps yield $\sim 15 k_B T$ and $\sim 10 k_B T$ energies, respectively.

We propose a minimal model consisting of three conformational states of gp17 (Fig. 4a). Before ATP binding, gp17 is in an Apo state (**A**) whose structure is not known. In the first step, ATP binds and provides the energy to drive the transition from the Apo state to the extended state (**E**), whereupon it binds to the DNA. In the second step, ATP is hydrolyzed to

ADP and P_i and gp17 transitions from the extended state to the compact state (C), and translocates the DNA by 2 bp. In the third step, ADP and P_i are released and the DNA is passed onto the next gp17 subunit in the motor ring (alternatively, P_i could be released earlier during the second step, as suggested by studies of the phage $\phi 29$ motor¹⁷). The original gp17 subunit goes back to the A state. This order of conformational-chemical transitions allows for the E \rightarrow C transition—that goes “downhill” in free energy, as observed from our free energy calculations, and requires no external energy—to occur during the ATP hydrolysis step that itself releases little or no energy²⁴. This then allows for the ATP binding and product release steps, the two energy-producing chemical transitions, to be utilized for pushing gp17 towards the energetically unfavorable extended state (A \rightarrow E) and releasing gp17 from its energetically favorable compact state (C \rightarrow A), respectively. This proposed G_{gp17} profile is shown in Fig. 4b-d as the red line. Note that based on our simulations we only know that G_{gp17} decreases during the E \rightarrow C transition, with free energy difference $G_{EC} \equiv G_{gp17}(C) - G_{gp17}(E) < 0$, and increases during the A \rightarrow E and C \rightarrow A transitions, possibly involving energy barriers, but the magnitudes of the free energy differences and the heights and locations of the energy barriers are not known.

The mechanical work W is given by the applied force F multiplied by the distance the DNA is translocated against the force. During the A \rightarrow E transition, $W = 0$, as there is no DNA packaging during this transition. During the E \rightarrow C transition, $W = F \cdot x$, where x is the distance the DNA moves during this transition. At the end of this transition, the net amount of work performed is $W = F \cdot x$, where $x = 2$ bp. No additional work is performed during the C \rightarrow A transition, and the work remains at $W = F \cdot x$. The resulting W profile is shown as the green line in Fig. 4b-d.

In the absence of a load force (Fig. 4b), the overall free energy profile G_{tot} (shown as the black line) exhibits a largely downhill path, potentially with energy barriers between each of the three conformational transitions, which facilitates efficient packaging of DNA. As described earlier, this is made possible by the constructive coupling between conformational and chemical transitions, which allows for efficient utilization of the energy released from ATP hydrolysis. Overall, each DNA translocation step of 2 bp leads to a net reduction in the free energy of the system (gp17 + solution) equal to the total free energy released by the hydrolysis of one ATP molecule, *i.e.*, $G_{ATP} \approx 25 k_B T$.

The observed reduction in the motor velocity with increasing load force F (Fig. 3b) suggests the presence of an energy barrier between the E and C states. The applied force, due to the mechanical work W , increases this barrier height by an amount $\sim F \cdot x^*$, where x^* is the location of the barrier relative to the E state along the force direction. Assuming an Arrhenius-like dependence in transition rates across barriers³⁸, the DNA translocation rate k_t (and hence the motor velocity) should then approximately decrease with increasing F via $k_t \propto \sim \exp[-(G^* + F \cdot x^*)/k_B T]$, where G^* denotes height of this energy barrier (Fig. 4c). However, based on our findings with gp17 mutants we propose that at sufficiently large F , the work term tilts the energy landscape between E and C states to such a large extent that the free energy of state C now becomes higher than that at the original barrier, making the crossing of state C the rate limiting step (Fig. 4d). The relevant barrier height then becomes

equal to the free energy difference between states **E** and **C**, as given by $G_{EC} + F \cdot x$. The rate of DNA translocation should consequently reduce via $k_t \propto \sim \exp[-(G_{EC} + F \cdot x)/k_B T]$.

Our measurements show that the mutant motors generate smaller packaging forces than WT motors. This effect can be understood based on our free-energy calculations, which predict the **E** \rightarrow **C** transition as being less favorable for mutants, leading to larger state **C** free energies for the mutants as compared to the WT motor, as depicted in Fig. 4b-d. In addition to having lower stall forces (<60 pN), the mutants also exhibit slower rates of packaging as compared to WT motors, and this difference becomes more significant at high loads. This can be explained by our model, which predicts that the rate of DNA translocation varies as $k_t \propto \exp[-(G^* + F \cdot x^*)/k_B T]$ at low loads and as $k_t \propto \exp[-(G_{EC} + F \cdot x)/k_B T]$ at high loads. That the mutants and WT motors exhibit smaller differences at low forces implies that they both exhibit similar energy barriers G^* (Fig. 4c). In contrast, the stronger effect of mutations on the packaging rate at high loads is consistent with the mutations decreasing the magnitude of G_{EC} (Fig. 4d).

The observed increase in pausing and slipping of DNA during translocation with high applied force and with mutations (Fig. 2) can also be explained by the energy landscape model. A recent study of T4 packaging at low ATP concentration suggested the presence of a pause-“unpackaging” state in the mechanochemical kinetic cycle that branches off from the DNA translocation pathway⁴². Our present results further suggest that with saturating ATP the motor can switch to this alternate pathway while residing at the **E** state under a high load force, which represents the most stretched conformation of the motor (Fig. 4a). It then follows that conditions slowing down the **E** \rightarrow **C** transition rate, such as the applied load and the residue changes studied here, would increase the time that the motor resides in the **E** state. This in turn increases the chances of the motor entering the proposed pause-unpackaging state, leading to increased rates of pausing and slipping, which is consistent with our observations.

Discussion

Using a combination of single-molecule measurements with applied forces, site-directed mutagenesis, and molecular dynamics simulations, we have quantitatively demonstrated the importance of electrostatic interactions between residues located at the interface of the N- and C-terminal subdomains of gp17 to mediate DNA translocation. These findings support the T4 motor force-generation mechanism proposed by Sun et al. on the basis of structural data²⁷. We show that our results with both WT and mutant motors under a wide range of load forces can be rationalized, at least qualitatively, by an energy landscape model that couples the free energy profile of motor conformational states with that of the ATP hydrolysis cycle.

Many molecular motors rely on large-scale structural rearrangements to forcibly translocate cargo. These rearrangements are often coupled to structural changes in the vicinity of the ATP binding pocket during the ATP hydrolysis cycle, which cause allosteric effects that may be leveraged to produce large-scale motions. Although coordination of multiple parallel electrostatic interactions across an interface between two subdomains has not been

previously demonstrated as a mechanism to directly produce motor force, evidence suggests that both myosin⁴³ and FoF1-ATP synthase⁴⁴ rely on electrostatic interactions between single pairs of charged residues to initiate structural transitions largely mediated by polar and hydrophobic interactions. As the T4 motor shares some features with many other ring-shaped nucleoside triphosphatases, including enzyme complexes involved in DNA replication and transcription (helicases), protein degradation, and chromosome segregation, the force generation mechanism investigated here may well have broader implications⁴⁵.

Methods

Materials—A 25,339 bpds DNA construct used as a substrate for packaging was prepared by PCR from lambda phage DNA (NEB, Inc.) using primers biotin-5'-CTGATGAGTTCGTGTCCGTACAACCTGGCGTAATC and 5'-ATCCGATCTGCGTTACCGAATGGATGGATG (Operon, Inc.) and the PCR Extender System (5 Prime, Inc.)³⁷.

T4 phage heads were purified from the 10am. 13am. hoc-del. soc-del phage mutant^{46,47} (*E. coli* P301 (sup-) cells infected with this mutant were lysed in Pi-Mg buffer (26 mM Na₂HPO₄, 68 mM NaCl, 22 mM KH₂PO₄, 1mM MgSO₄, pH 7.5) containing 10 µg/ml DNase I and chloroform and incubated at 37°C for 30 min. The lysate was subjected to two low (6,000 x g for 10 min) and high (35,000 x g for 45min) speed centrifugations and the final heads pellet was resuspended in Tris-Mg buffer (10 mM Tris-HCl, pH 7.5, 50 mM NaCl and 5 mM MgCl₂) and purified by CsCl density gradient centrifugation. The major head band sedimented at about 1/3rd from the bottom of a 5 ml gradient was extracted and dialyzed overnight against Tris-Mg buffer. The heads were further purified by DEAE-Sephadex ion-exchange chromatography. The peak heads fractions were concentrated and stored at -80°C.

Wild-type and mutant gp17 motor proteins were purified from *E. coli* BL21 (DE3) RIPL cells harboring the recombinant clones^{46,47}. The recombinant proteins were over-expressed with 1 mM IPTG for 2 h at 30°C. The cells were harvested by centrifugation (4,000 x g for 15 min at 4°C) and resuspended in HisTrap binding buffer (50 mM Tris HCl, pH 8.0, 20 mM imidazole, and 300 mM NaCl). The cells were lysed using French-press (Aminco, USA) and the soluble fraction containing the His-tagged fusion protein was isolated by centrifugation at 34,000 x g for 20 min. The supernatant was loaded onto a HisTrap column (GE Healthcare), washed with 50mM imidazole containing buffer and the protein was eluted with 20-500 mM linear imidazole gradient. The peak fractions were concentrated and purified by size exclusion chromatography using Hi-Load 16/60 Superdex-200 (pre-graded) gel filtration column (GE Healthcare) in a buffer containing 20 mM Tris-HCl, pH 8.0 and 100 mM NaCl. The peak fractions were concentrated and stored at -80°C.

Bulk DNA packaging assays—DNase protection assays shown in Supplemental Fig. 2 were performed as follows⁴⁸. The purified wild-type or mutant gp17 proteins were incubated with phage heads in the presence of 30mM Tris-HCl (pH 7.5), 100 mM NaCl, 3 mM MgCl₂, 1 mM ATP, and phage λ DNA (48.5 kb) for 30 minutes at 37°C. DNase I (Sigma) was added to terminate DNA packaging and digest the unprotected DNA.

Proteinase K (0.5 $\mu\text{g}/\mu\text{l}$), 50 mM EDTA, and 0.2% SDS were added and incubated for 30 minutes at 65°C to digest DNase I and capsid and release the packaged DNA. The samples were electrophoresed on 0.8 % (w/v) agarose gel for 2-3 h at 100 V and DNA was stained with ethidium bromide.

Single-molecule packaging measurements—T4 head-motor complexes were prepared by mixing 1.7×10^{10} heads with 70 picomols of gp17 in a solution containing 50 mM Tris-HCl pH 7.5, 5 mM MgCl_2 , 80 mM NaCl, 1 mM gamma-S-ATP (non-hydrolyzable ATP analog), and 450 ng of 120 bp “initiating” DNA (which we found stabilizes the competent head-motor complex)¹⁴. This solution was incubated at room temperature for 45 min. 2 μl of T4 antibody coated 2.2 μm diameter protein-G microspheres (Spherotech) were mixed 10 μl of these stalled T4 complexes and incubated at room temperature for 45 min. The biotinylated DNA was attached to 2.2 μm diameter streptavidin coated microspheres (Spherotech). Measurements were carried out in solution containing 50 mM Tris-HCl pH 7.5, 5 mM MgCl_2 , 80 mM NaCl, 1 mM ATP, and 0.05 g/L BSA.

High force measurements—Packaging was first measured at low force (5 pN) for 5-10 seconds in force clamp mode¹⁴, to verify motor activity. The force was then quickly ramped (within 0.2 s) to a higher value by adjusting the set-point on the force-clamp control system. DNA translocation (packaging and/or slipping) was then tracked in force-clamp mode until the DNA tether was lost. The force was monitored at 2 kHz and was held constant by a feedback control system that adjusts the separation between the two traps in 0.5 nm increments. The optical tweezers system was calibrated as described previously^{49,50}.

Data Analysis—The motor velocity was calculated using methods similar as those described previously¹⁴ by linear fitting of the DNA length vs. time records in a 1 s sliding window. Slips larger than 100 bp and pauses in which the velocity dropped to <12 bp/s in the 1 s window were not included in determining “motor velocity” (but were included in determining overall “packaging rate”).

Computational Methods

Overview—Our aim is to compute the free energy difference $G_{\text{EC}} \equiv G_{\text{C}} - G_{\text{E}}$ between the extended and compact states of gp17 for the wild type and mutant proteins. In principle, G_{EC} can be computed from all-atom molecular dynamics (MD) simulations via approaches like umbrella sampling, though such approaches would entail prohibitive computational costs for systems as large as gp17. To this end, we use the Molecular Mechanics-Generalized Born Surface Area (MM-GBSA) method³⁹, which provides quick estimates of the binding free energy of molecular complexes by approximating the solvation free energy using implicit solvent mean field models. However, the application of MM-GBSA to computing intramolecular binding free energies, as opposed to intermolecular binding free energies, requires the N- and C-terminal domains to be treated as separate “molecules”, which assumes, consistent with structural features observed in Ref. that the hinge joining the two domains is flexible and does not contribute much to the free energy difference between the compact and extended states. One can then obtain G_{EC} using the free energy cycle shown in Supplemental Fig. 3, where the MM-GBSA method is used to compute the binding

free energies $G_{\text{bind,E}}$ and $G_{\text{bind,C}}$ for assembling the N- and C-terminal domains into extended and compact states from a common isolated state in which the two domains do not interact with each other. The required free energy difference can then be simply calculated as $G_{\text{EC}} = G_{\text{bind,E}} - G_{\text{bind,C}}$.

Preparation of initial configurations—The MM-GBSA method involves all-atom MD simulations of the extended and compact state complexes in explicit solvent and ions, starting from suitable initial configurations. These initial configurations were prepared based on the high-resolution crystal structure of gp17 in the compact state (PDB code: 3CPE)²⁷.

To generate the initial configuration of the compact state complex, we solvated the crystal structure in a TIP3P water box extending 10 Å from the surface of the protein in each direction by using the *solvate* function in VMD and then added 150 mM NaCl by using the *autoionize* function in VMD⁵¹. The solvated structure was energy minimized using 100 steps of steepest gradient, and then equilibrated using MD simulations for 0.5 ns to yield the initial configuration of the compact state complex. The atomic structure of the extended state is not known from X-ray studies but the cryo-electron microscopy studies show that the C- and N-terminal domains are spaced a further ~7 Å apart as compared to the compact state²⁷. To generate an atomic model of this state we generated a vector between the center of mass of the N- and C-terminal domains and used steered MD simulations to pull the C-terminal domain along this vector at a slow rate of 0.0002 Å/fs until a separation of 7 Å between the two center of masses was achieved. The resulting structure was equilibrated using MD simulations for 0.5 ns.

To generate the extended and compact state complexes for the three studied mutants, we used the *mutator* function in VMD to replace the chosen residue with the desired residue in the final equilibrated complexes. We then carried out 100 steps of energy minimization via steepest descent to allow the mutated residue as well as the nearby residues and water molecules to relax to their low-energy conformations.

Energy minimization and MD simulations used for preparing the initial configurations were performed in NAMD⁵² using the CHARMM 27 force field⁵³. The simulations were carried out at constant temperature and pressure consistent with physiological conditions. The temperature was maintained at 310 K using a Langevin thermostat with a damping constant 1/ps and the pressure was maintained at 1 atm using a Langevin piston with a period of 100 fs and damping time constant of 50 fs. We used a time step of 2 fs for integrating the equations of motion and employed the SHAKE algorithm to constrain all bond lengths involving hydrogen atoms. For computing short-range non-bonded interactions, a cutoff distance of 12 Å was employed. The simulations were carried out with periodic boundary conditions with all electrostatic interactions computed using the particle mesh Ewald method with grid spacing of 1 Å.

We generated three additional initial configurations of the complexes by performing MD simulations of the original initial configurations described above. These additional simulations were carried out at three different temperatures (300 K, 320 K, and 330 K) for 50 ps while imposing a weak restraint on all heavy atoms of the protein via a harmonic

potential with a spring constant of 2.0 kcal/mol/Å². This procedure forced the configurations to depart significantly from the starting configuration while remaining stable at these non-physiological temperatures. We carried out a further 600 ps of MD simulations during which the restraints were removed and the temperatures were brought back to 310 K. Thus, a total of four different initial configurations for each complex were obtained, allowing us to carry out four independent MM-GBSA calculations for improving the accuracy of our free energy estimates.

MM-GBSA calculations—We next performed exhaustive MD simulations of extended state and compact state complexes for wild type and mutant gp17. The binding free energies

$G_{\text{bind,E}}$ and $G_{\text{bind,C}}$ were computed according to MM-GBSA via the following relation: $G_{\text{bind}} = E_{\text{MM}} + G_{\text{solv}} - T S_{\text{conf}}$, where E_{MM} , G_{solv} , and $T S_{\text{conf}}$ represent respective changes in molecular mechanics energy, solvation free energy, and configurational entropy of the C- and N-terminal domains as they associate into a complex (extended or compact).

The three free energy contributions were computed from 500 snapshots of each complex recorded during 4 ns MD simulations, carried out using the *mm_pbsa.pl* script in AMBER 10⁵⁴. In these calculations, we defined the N- and C-terminal domains as separate molecules, namely, the “receptor” and “ligand”, respectively, and the full-length gp17 molecule as the “complex”, as explained earlier. Since the flexible hinge region contains residues 358–362, we define the N- and C-terminal domains by residues 1–359 and 360–560, respectively. The E_{MM} contributions were directly computed as the change in the sum of the bonded, electrostatic, and vdW interaction energies. The G_{solv} contributions were further divided into polar and nonpolar contributions. The polar contributions were calculated using the Generalized Born approach^{55,56} while the nonpolar contributions were calculated from changes in solvent accessible surface area upon binding multiplied by the surface tension³⁴. We used a water probe of radius 1.4 Å and a surface tension of 0.0072 kcal/mol/Å² for the latter calculation. The $T S_{\text{conf}}$ contributions are typically computed using normal mode analysis³⁵, but these calculations were found to converge extremely slowly. Hence, we neglected its contributions to the free energy difference. However, we believe that these entropic contributions will mostly cancel out when comparing G_{EC} values across wild type and mutant gp17. The algorithms and associated parameters, force field, and external conditions used for these MD simulations were kept identical to those used for generating the initial conditions.

To obtain reliable values of G_{EC} as well as statistical uncertainties, we carried out four sets of MM-GBSA calculations for each wild type and mutant complex, each starting from the four different initial configurations of the extended and compact state complex prepared using the procedures described in the previous section.

Supplementary Material

Refer to Web version on PubMed Central for supplementary material.

Acknowledgments

This work was supported by NIH grant R01-GM088186 (to DES), NSF grant PHY-0848905 (to DES), NSF grant MCB-0923873 (to VBR) and, in part, by NIH grant R01AI081726 (to VBR).

References

1. Smith DE, et al. The bacteriophage phi29 portal motor can package DNA against a large internal force. *Nature*. 2001; 413:748–752. [PubMed: 11607035]
2. Jardine, PJ.; Anderson, DL. DNA Packaging in dsDNA Phages. In: Calendar, R., editor. *The Bacteriophages*. 2nd. Oxford University Press; New York, NY: 2006.
3. Feiss, M.; Rao, VB. The bacteriophage DNA packaging machine. In: Rao, V.; Rossmann, MG., editors. *Viral Molecular Machines*. Springer; New York, NY: 2012. p. 489-509.
4. Morais, MC. The dsDNA packaging motor in bacteriophage ϕ 29. In: Rao, V.; Rossmann, MG., editors. *Viral Molecular Machines*. Springer; New York, NY: 2012. p. 511-547.
5. Smith DE. Single-molecule studies of viral DNA packaging. *Curr Opin Virol*. 2011; 1:134. [PubMed: 22440623]
6. Chemla, YR.; Smith, DE. Single-molecule studies of viral DNA packaging. In: Rao, V.; Rossmann, MG., editors. *Viral Molecular Machines*. Springer; New York, NY: 2012. p. 549-584.
7. Tzllil S, Kindt JT, Gelbart WM, Ben-Shaul A. Forces and pressures in DNA packaging and release from viral capsids. *Biophys J*. 2003; 84:1616–1627. [PubMed: 12609865]
8. Purohit PK, et al. Forces during bacteriophage DNA packaging and ejection. *Biophys J*. 2005; 88:851–866. [PubMed: 15556983]
9. Fuller DN, et al. Ionic effects on viral DNA packaging and portal motor function in bacteriophage phi 29. *Proc Natl Acad Sci U S A*. 2007; 104:11245–11250. [PubMed: 17556543]
10. Harvey SC, Petrov AS, Devkota B, Boz MB. Viral assembly: a molecular modeling perspective. *Phys Chem Chem Phys*. 2009; 11:10553–10564. [PubMed: 20145801]
11. Berndsen ZT, Keller N, Grimes S, Jardine PJ, Smith DE. Nonequilibrium dynamics and ultra-slow relaxation of confined DNA during viral packaging. *Proc Natl Acad Sci USA*. 2014 in press.
12. Keller N, delToro D, Grimes S, Jardine PJ, Smith DE. Repulsive DNA-DNA interactions accelerate viral DNA packaging in phage phi29. *Phys Rev Lett*. 2014 in press.
13. Fuller DN, et al. Measurements of single DNA molecule packaging dynamics in bacteriophage lambda reveal high forces, high motor processivity, and capsid transformations. *J Mol Biol*. 2007; 373:1113–1122. [PubMed: 17919653]
14. Fuller DN, Raymer DM, Kottadiel VI, Rao VB, Smith DE. Single phage T4 DNA packaging motors exhibit large force generation, high velocity, and dynamic variability. *Proc Natl Acad Sci U S A*. 2007; 104:16868–16873. [PubMed: 17942694]
15. Rickgauer JP, et al. Portal motor velocity and internal force resisting viral DNA packaging in bacteriophage phi29. *Biophys J*. 2008; 94:159–167. [PubMed: 17827233]
16. Chemla YR, et al. Mechanism of force generation of a viral DNA packaging motor. *Cell*. 2005; 122:683–692. [PubMed: 16143101]
17. Moffitt JR, et al. Intersubunit coordination in a homomeric ring ATPase. *Nature*. 2009; 457:446–450. [PubMed: 19129763]
18. Chistol G, et al. High degree of coordination and division of labor among subunits in a homomeric ring ATPase. *Cell*. 2012; 151:1017–1028. [PubMed: 23178121]
19. Rao VB, Feiss M. The Bacteriophage DNA Packaging Motor. *Annu Rev Genet*. 2008; 42:647–681. [PubMed: 18687036]
20. Mitchell MS, Matsuzaki S, Imai S, Rao VB. Sequence analysis of bacteriophage T4 DNA packaging/terminase genes 16 and 17 reveals a common ATPase center in the large subunit of viral terminases. *Nucleic Acids Res*. 2002; 30:4009–4021. [PubMed: 12235385]
21. Iyer LM, Leipe DD, Koonin EV, Aravind L. Evolutionary history and higher order classification of AAA+ ATPases. *J Struct Biol*. 2004; 146:11–31. [PubMed: 15037234]

22. Tsay JM, Sippy J, Feiss M, Smith DE. The Q motif of a viral packaging motor governs its force generation and communicates ATP recognition to DNA interaction. *Proc Natl Acad Sci U S A*. 2009; 106:14355–14360. [PubMed: 19706522]
23. Tsay JM, et al. Mutations altering a structurally conserved loop-helix-loop region of a viral packaging motor change DNA translocation velocity and processivity. *J Biol Chem*. 2010; 285:24282–24289. [PubMed: 20525695]
24. Oster G, Wang H. Reverse engineering a protein: the mechanochemistry of ATP synthase. *Biochim Biophys Acta*. 2000; 1458:482–510. [PubMed: 10838060]
25. Liu H, Shi Y, Chen XS, Warshel A. Simulating the electrostatic guidance of the vectorial translocations in hexameric helicases and translocases. *Proc Natl Acad Sci U S A*. 2009; 106:7449–7454. [PubMed: 19383795]
26. Mukherjee S, Warshel A. Electrostatic origin of the mechanochemical rotary mechanism and the catalytic dwell of F1-ATPase. *Proc Natl Acad Sci U S A*. 2011; 108:20550–20555. [PubMed: 22143769]
27. Sun S, et al. The Structure of the Phage T4 DNA Packaging Motor Suggests a Mechanism Dependent on Electrostatic Forces. *Cell*. 2008; 135:1251–1262. [PubMed: 19109896]
28. Morita M, Tasaka M, Fujisawa H. Structural and functional domains of the large subunit of the bacteriophage T3 DNA packaging enzyme: importance of the C-terminal region in prohead binding. *J Mol Biol*. 1995; 245:635–644. [PubMed: 7844832]
29. Dixit AB, Ray K, Thomas JA, Black LW. The C-terminal domain of the bacteriophage T4 terminase docks on the prohead portal clip region during DNA packaging. *Virology*. 2013; 446:293–302. [PubMed: 24074593]
30. Hegde S, Padilla-Sanchez V, Draper B, Rao VB. Portal-large terminase interactions of the bacteriophage T4 DNA packaging machine implicate a molecular lever mechanism for coupling ATPase to DNA translocation. *J Virol*. 2012; 86:4046–4057. [PubMed: 22345478]
31. Ray K, Sabanayagam CR, Lakowicz JR, Black LW. DNA crunching by a viral packaging motor: Compression of a procapsid-portal stalled Y-DNA substrate. *Virology*. 2010; 398:224–232. [PubMed: 20060554]
32. Catalano, CE., editor. *Viral Genome Packaging Machines: Genetics, Structure, and Mechanism*. Kluwer Academic/Plenum Press; New York, NY: 2005.
33. Lebedev AA, et al. Structural framework for DNA translocation via the viral portal protein. *EMBO J*. 2007; 26:1984–94. [PubMed: 17363899]
34. Yu J, Moffitt J, Hetherington CL, Bustamante C, Oster G. Mechanochemistry of a viral DNA packaging motor. *J Mol Biol*. 2010; 400:186–203. [PubMed: 20452360]
35. Serwer P, Jiang W. Dualities in the analysis of phage DNA packaging motors. *Bacteriophage*. 2012; 2:239. [PubMed: 23532204]
36. Zhao H, Christensen TE, Kamau YN, Tang L. Structures of the phage Sf6 large terminase provide new insights into DNA translocation and cleavage. *Proc Natl Acad Sci U S A*. 2013; 110:8075–8080. [PubMed: 23630261]
37. Fuller DN, et al. A general method for manipulating DNA sequences from any organism with optical tweezers. *Nucleic Acids Res*. 2006; 34:e15. [PubMed: 16452295]
38. Keller D, Bustamante C. The mechanochemistry of molecular motors. *Biophys J*. 2000; 78:541–556. [PubMed: 10653770]
39. Massova I, Kollman PA. Combined molecular mechanical and continuum solvent approach (MM-PBSA/GBSA) to predict ligand binding. *Perspect Drug Discov Des*. 2000; 18:113–135.
40. Sun S, Kondabagil K, Gentz PM, Rossmann MG, Rao VB. The structure of the ATPase that powers DNA packaging into bacteriophage t4 procapsids. *Mol Cell*. 2007; 25:943–949. [PubMed: 17386269]
41. Singh N, Warshel A. Absolute binding free energy calculations: On the accuracy of computational scoring of protein–ligand interactions. *Proteins Structure Function and Bioinformatics*. 2010; 78:1705–1723.
42. Kottadiel VI, Rao VB, Chemla YR. The dynamic pause-unpackaging state, an off-translocation recovery state of a DNA packaging motor from bacteriophage T4. *Proc Natl Acad Sci U S A*. 2012; 109:20000–20005. [PubMed: 23169641]

43. Fischer S, Windshügel B, Horak D, Holmes KC, Smith JC. Structural mechanism of the recovery stroke in the myosin molecular motor. *Proc Natl Acad Sci U S A*. 2005; 102:6873–6878. [PubMed: 15863618]
44. Ito Y, Oroguchi T, Ikeguchi M. Mechanism of the conformational change of the F1-ATPase β subunit revealed by free energy simulations. *J Am Chem Soc*. 2011; 133:3372–3380. [PubMed: 21341660]
45. Allemand J, Maier B, Smith DE. Molecular motors for DNA translocation in prokaryotes. *Curr Opin Biotechnol*. 2012; 23:503–509. [PubMed: 22226958]
46. Zhang Z, et al. A promiscuous DNA packaging machine from bacteriophage T4. *PLoS Biol*. 2011; 9:e1000592. [PubMed: 21358801]
47. Tao P, et al. In vitro and in vivo delivery of genes and proteins using the bacteriophage T4 DNA packaging machine. *Proc Natl Acad Sci U S A*. 2013; 110:5846–5851. [PubMed: 23530211]
48. Kondabagil KR, Zhang Z, Rao VB. The DNA translocating ATPase of bacteriophage T4 packaging motor. *J Mol Biol*. 2006; 363:486–499.
49. Rickgauer JP, Fuller DN, Smith DE. DNA as a metrology standard for length and force measurements with optical tweezers. *Biophys J*. 2006; 91:4253–4257. [PubMed: 16963512]
50. delToro D, Smith DE. Accurate measurement of force and displacement with optical tweezers using DNA molecules as metrology standards. *Appl Phys Lett*. 2014; 104:143701. [PubMed: 25316922]
51. Phillips, J.; Isgro, T.; Sotomayor, M.; Villa, E. [accessed 6/2013] NAMD TUTORIAL. <http://www.ks.uiuc.edu/Training/Tutorials/namd/namd-tutorial-html/>
52. Nelson MT, et al. NAMD: a parallel, object-oriented molecular dynamics program. *Intl J High Perf Comput Applic*. 1996; 10:251–268.
53. MacKerell AD, Banavali N, Foloppe N. Development and current status of the CHARMM force field for nucleic acids. *Biopolymers*. 2000; 56:257–265. [PubMed: 11754339]
54. Pearlman DA, et al. AMBER, a package of computer programs for applying molecular mechanics, normal mode analysis, molecular dynamics and free energy calculations to simulate the structural and energetic properties of molecules. *Comput Phys Commun*. 1995; 91:1–41.
55. Onufriev A, Bashford D, Case DA. Exploring protein native states and large-scale conformational changes with a modified generalized born model. *Proteins Structure Function and Bioinformatics*. 2004; 55:383–394.
56. Karplus M, Ichiye T, Pettitt B. Configurational entropy of native proteins. *Biophys J*. 1987; 52:1083–1085. [PubMed: 3427197]

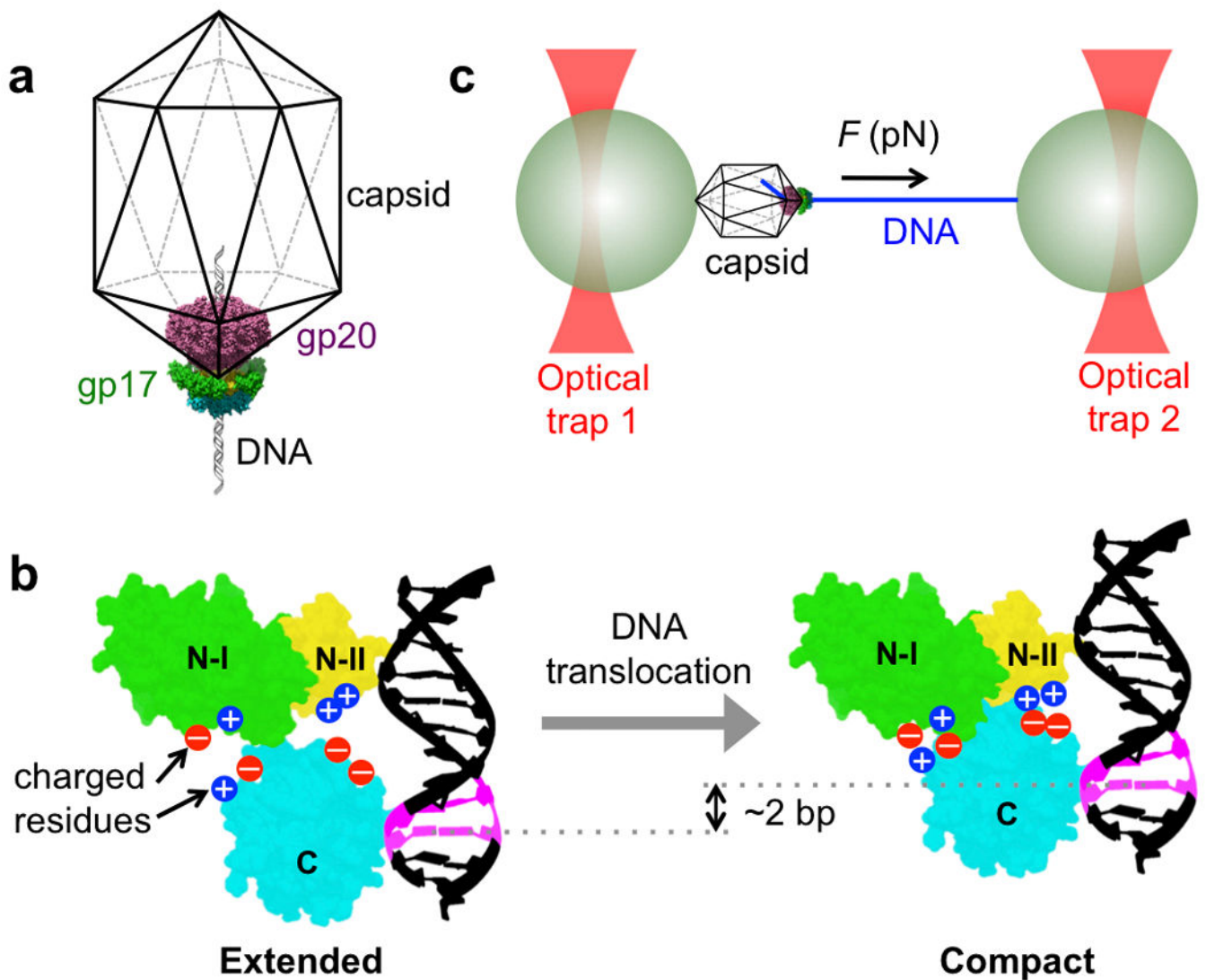


Fig. 1. Schematic overview of the T4 packaging motor structure and the single-molecule measurement technique

(a) The T4 packaging motor consists of concentric rings of gp17 (motor) and gp20 (portal) proteins at the special five-fold vertex of the viral capsid. (b) Structural data indicates that gp17 can adopt extended (left) and compact states (right). The X-ray structure shows a large interface between the N-terminal (composed of two sub-regions, N-I and N-II) and C-terminal globular subdomains containing pairs of apparently aligned complimentary charged residues. The electrostatic force model²⁷ proposes that attractive interactions between these residues generates the force during a conformational change from the extended to the compact state that translocates the DNA into the capsid in steps of ~ 2 bp. (c) Dual optical tweezers are used to measure the packaging of single DNA molecules into single capsid-motor complexes under applied load forces.

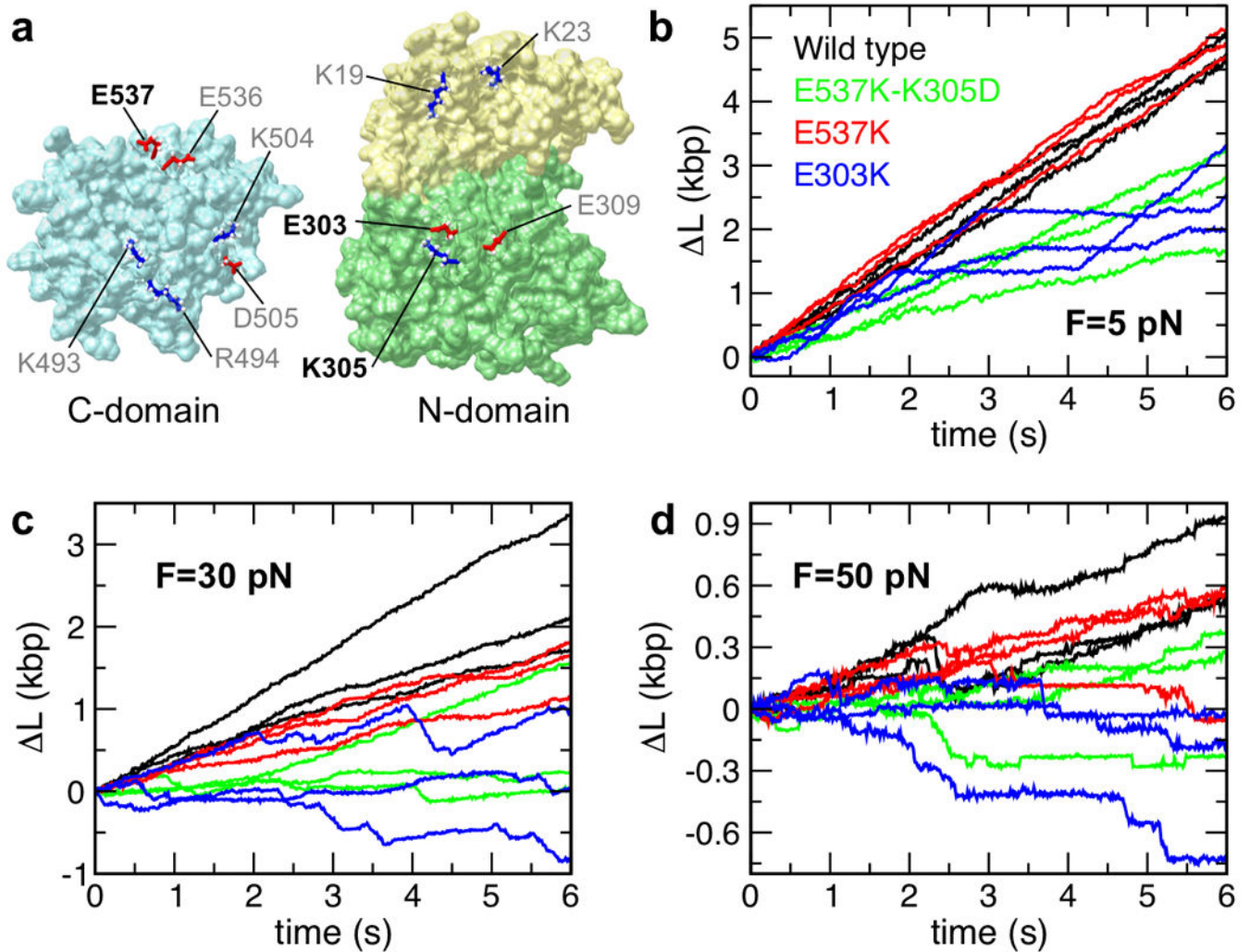


Fig. 2. Locations of altered charged residues and measurements of DNA packaging dynamics (a) Open book representation of the N- and C-terminal domains of gp17 (PDB ID code 3CPE) displaying the charged residues studied in this work. Changes in the residues labeled in grey resulted in zero bulk packaging while those labeled in black resulted in some packaging, leading to their further study through optical traps. Red indicates acidic interface residues, while blue indicates basic interface residues. (b-d) Representative measurements of single DNA molecule packaging dynamics (length packaged vs. time) with (b) 5 pN applied load, (c) 30 pN, (d) 50 pN. The colors indicate WT (black), E537K (red), E537K-K305D (green), and E303K (blue) gp17 motors.

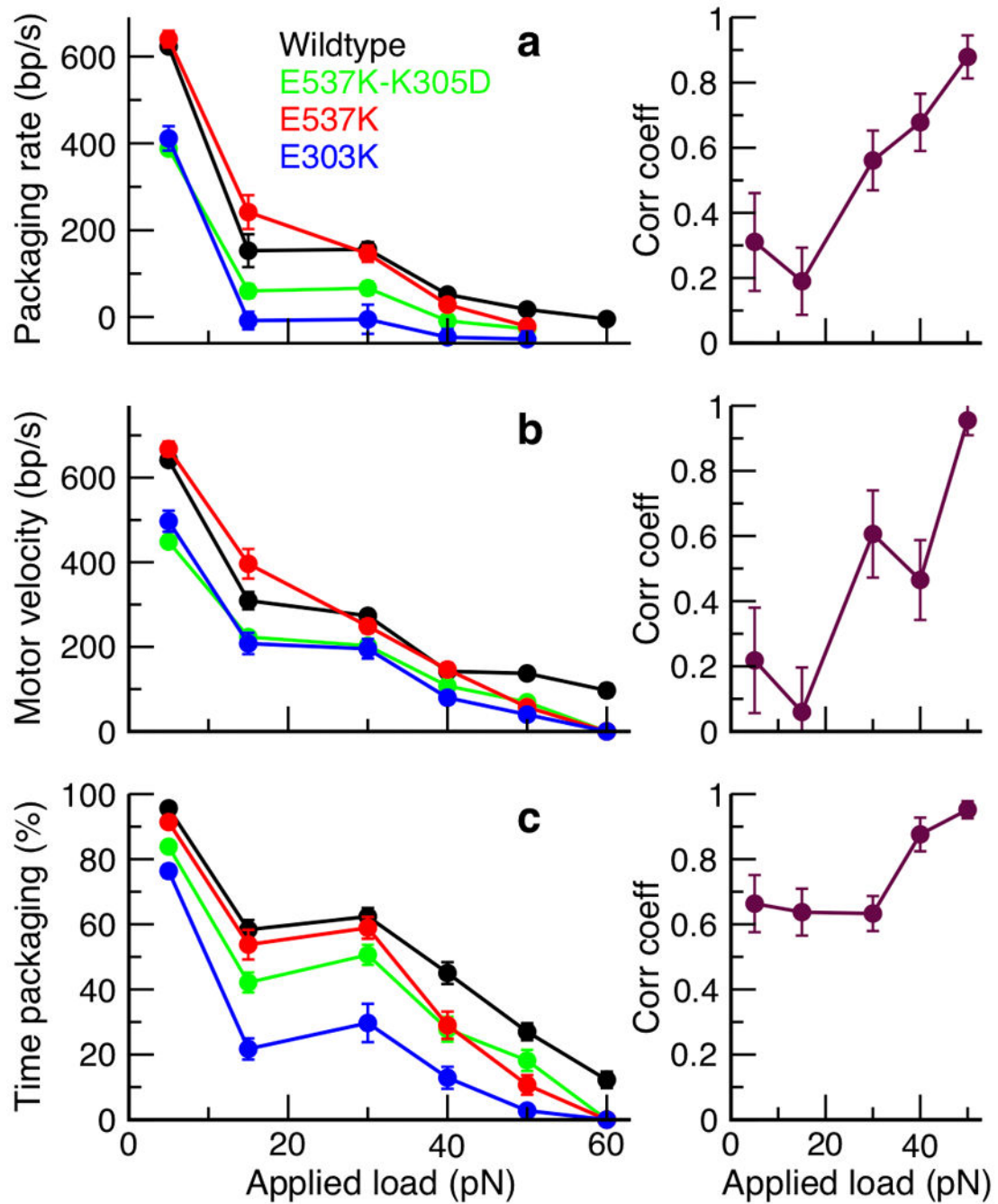


Fig. 3. Experimental metrics of motor activity and correlation with computed free-energy changes in gp17

(a-c, left panel) Average measured packaging rate **(a)**, motor velocity **(b)**, and % time spent packaging **(c)** for wild type gp17 (black), E537K (red), E537K-K305D (green), E303K (blue). The number of independent packaging events measured for each complex is given in Supplemental Table 1, and the error bars indicate standard error of the means. **(a-c, right panel)** corresponding Pearson correlation coefficients (min=0, max=1) between experimental metrics of motor function (adjacent plots) and calculated free energy changes

between the extended and compact forms of gp17. The error bars indicate standard error of the means.

Author Manuscript

Author Manuscript

Author Manuscript

Author Manuscript

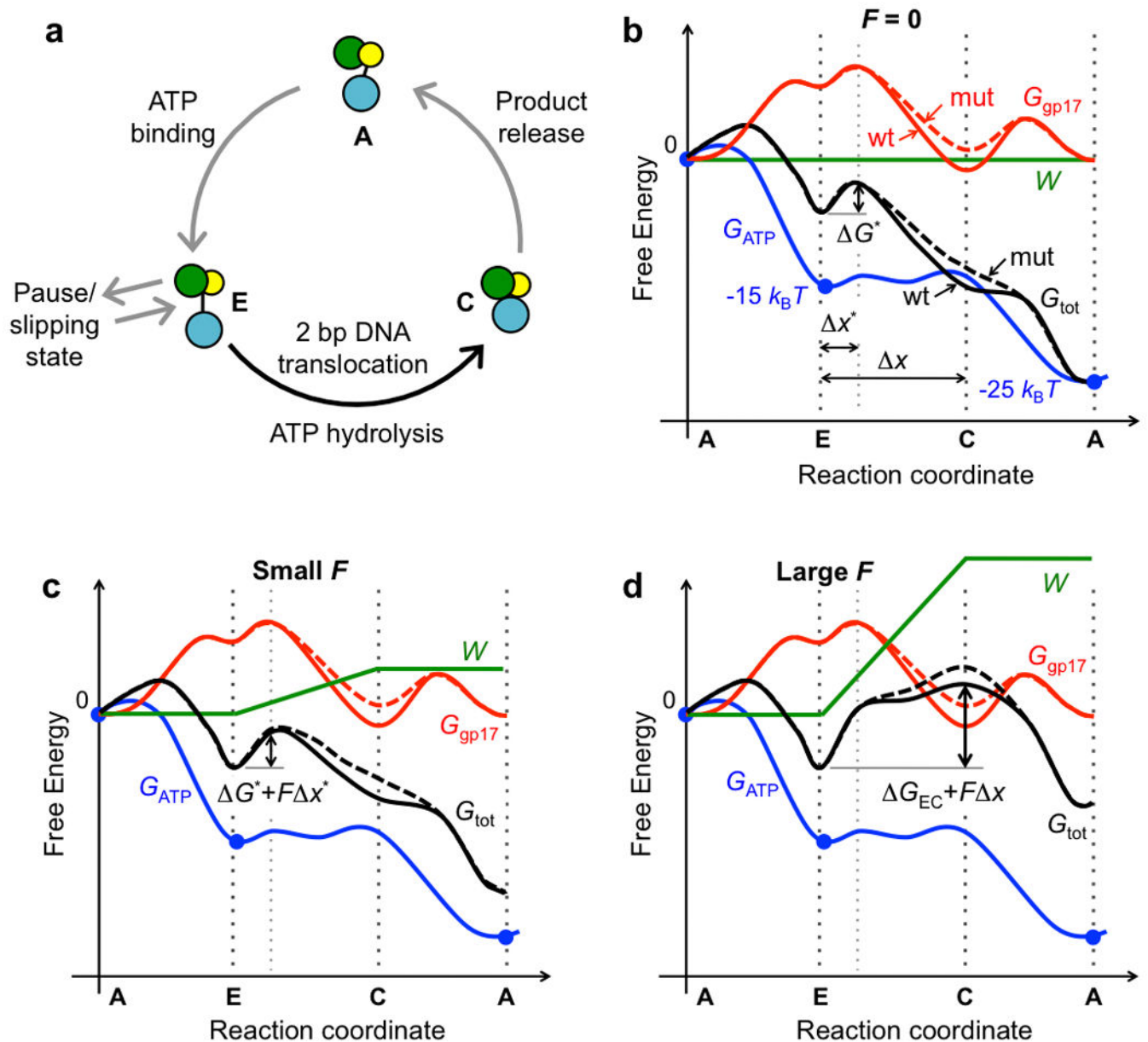


Fig. 4. Mechanochemical energy landscape model inferred from experimental and computational findings

(a) Proposed coupling between conformational transitions in gp17 and chemical transitions in ATP during a 2 bp DNA translocation cycle driven by the hydrolysis of one ATP molecule. The pausing and slippage of DNA is represented as an alternative state branching off from and rejoining at the extended state of gp17. (b-d) The conformational energy landscape of gp17 (red line), the ATP hydrolysis free energy profile (blue line), and mechanical work (green line) add up to yield the overall mechanochemical energy landscapes (black line). The shapes of the different energy landscape are schematically drawn for three cases: zero load (b), small load (c), and large applied loads (d).